Journal of Science and Transport Technology
Journal homepage: https://jstt.vn/index.php/en

UNIVERSITY OF TRANSPORT TECHNOLOGY

Experimental–Numerical Analysis of the Ultimate Lateral Capacity of PHC Piles

Vo Nhat Luan[1], Van Quang Nguyen[2*], Thi Thanh Huong Ngo[2], Quynh-Anh Thi Bui[2], Do Ngoc Thai[3]
[1]Van Hien University, Ho Chi Minh 70000, Vietnam
[2]University of Transport Technology, Hanoi 100000, Vietnam
[3]Hanoi University of Mining and Geology, Hanoi 100000, Vietnam

Article info
Type of article:
Original research paper

DOI:
https://doi.org/10.58845/jstt.utt.2026.en.6.3.58-76

[*]**Corresponding author:**
Email address:
quangnv@utt.edu.vn

Received: 19/03/2025
Received in Revised Form: 11/06/2026
Accepted: 23/06/2026

Abstract: This study investigates the ultimate lateral behavior of prestressed high-strength concrete (PHC) piles in layered ground conditions at a thermal power plant site in Nhon Trach, Vietnam. Full-scale free-head lateral load tests were conducted on single PHC piles with diameters of 300, 400, and 500 mm, and the measured load–displacement responses were used to calibrate a three-dimensional finite element model in Plaxis 3D. The calibrated model reproduced the experimental H–u curves with good agreement and was further used to examine the effects of soil stratification and head boundary conditions. Comparison with the Japanese Road Association (JRA) analytical approach shows that JRA provides conservative displacement predictions for the larger-diameter piles (D400–D500) over practical displacement ranges, while the agreement improves for D300 at larger deformations, reflecting the stronger influence of the underlying soft clay and the limitations of equivalent-soil idealizations in layered profiles. Normalized head displacements at maximum test loads fall within u/D≈0.06–0.13, consistent in order of magnitude with reported full-scale lateral pile tests in the literature. The results support using JRA for rapid screening, whereas calibrated 3D numerical analysis is recommended for working design and for translating free-head test outcomes to fixed-head or pile-group boundary conditions in similar layered ground settings.

Keywords: PHC piles, lateral capacity, FEM, loading condition.

1. Introduction

Precast High-Strength Concrete (PHC) piles are widely utilized in foundation engineering due to their superior mechanical performance, high durability, and economic efficiency. These piles are particularly favored in infrastructure projects such as high-rise buildings, bridges, and industrial facilities, especially in areas with poor ground conditions requiring enhanced load-bearing capacity. Among the different loading modes, the lateral load behavior of PHC piles is of critical concern in engineering design, particularly for structures exposed to wind, seismic events, or machine-induced vibrations. In thermal power plants, steam and gas turbines generate substantial lateral forces due to operational dynamics, thermal expansion, and seismic activities. The foundation systems for such installations must be carefully designed to withstand these lateral loads while ensuring long-term serviceability. However, accurately predicting the lateral capacity of PHC piles remains a technical challenge, primarily due to the complexity of soil–structure interaction and variability in subsurface conditions [1].

Numerous studies have explored the lateral behavior of piles through experimental investigations, analytical formulations, and advanced numerical simulations. Early foundational work by Hetényi [2] and Vesić [3] introduced the concept of the Winkler foundation model, providing a basis for understanding soil-pile interaction through idealized spring models. This was further enhanced by Matlock [4], and Reese et al. [5] who developed nonlinear p-y curve (unit lateral soil reaction - lateral displacement) methodologies to better represent soil resistance under lateral loading, especially for cohesionless and cohesive soils respectively. These models remain widely used in modern design codes and form the backbone of many analytical approaches.

Experimental studies have provided crucial insights into pile behavior under lateral loads. For instance, Zeng et al. [6] and Shengnan et al. [7] conducted large-scale tests on prestressed high-strength concrete (PHC) piles, revealing significant nonlinear lateral responses and stiffness degradation at high load levels. Their findings highlight the limitations of purely elastic models in capturing pile-soil behavior beyond service-level loading. Similarly, Zhou and Oh [8] carried out full-scale field tests which confirmed that lateral resistance is strongly governed by pile diameter, embedded depth, and the nature of surrounding soil layers, especially in layered or heterogeneous profiles.

In recent years, finite element analysis (FEA) has gained prominence due to its capacity to model complex soil behavior and boundary conditions. Studies by Li et al. [9] and Zeng and Ahmani [10] effectively utilized p-y curve-based formulations within FEA frameworks to simulate nonlinear soil resistance for both cohesive and cohesionless soils, aligning well with field observations. Their work demonstrates how advanced numerical tools can capture nuances such as gapping, strain softening, and cyclic degradation, which are often neglected in simpler analytical models.

Despite extensive advances in lateral pile analysis, two practice-critical features remain underrepresented in field-calibrated studies: (i) layered ground with a stiff sand cap over soft clay, common at large energy facilities; and (ii) fixed-head boundary conditions imposed by stiff pile caps that suppress pile-head rotation. These jointly govern service-level stiffness and bending demand, yet are seldom examined together at field scale with calibrated 3D models. Prior work largely targets free-head piles and/or homogeneous profiles, limiting direct transfer to fixed-head pile groups in layered soils.

This study (1) analyzes the lateral response of fixed-head PHC piles using advanced 3D finite-element modeling; (2) validates the numerical predictions against full-scale lateral load tests; and (3) evaluates how soil layering (stiff sand cap over soft clay) and pile configuration/diameter influence lateral resistance. The investigation focuses on fixed-head PHC pile groups installed in a stratified profile representative of the Nhon Trach 3&4 power-plant site, comprising ~3 m of sand backfill over ~10 m of soft clay.

This work focuses on lateral loading under predominantly static conditions in a layered deposit typical of Nhon Trach (≈3 m stiff sand cap over ≈10 m soft clay) with fixed-head restraint provided by a rigid cap. Axial–lateral interaction and cyclic/dynamic effects are not included in the baseline analysis. Model calibration and validation are performed against full-scale free-head tests using (i) the head load–displacement curve (H–u) including the initial tangent slope, and (ii) the crack-initiation load H_{cr}; design comparisons also consider the maximum bending moment Mmax and normalized displacement u/D. These definitions and the boundary-condition translation protocol (free-head → fixed-head/group) are used consistently throughout.

The contribution is threefold (1) A design-oriented framework is developed to translate evidence from free-head tests to fixed-head/group performance in layered soils via a calibrated Plaxis 3D model, so that practical test setups can be used reliably for fixed-head design. (2) Conditions under which code-type predictions (e.g., JRA) become conservative for larger-diameter PHC piles (D400–D500) due to the stiff sand cap while remaining approximately accurate for smaller diameters (D300) are quantified. (3) Compact, theory-consistent relations are provided, clarifying sensitivity: head displacement is shown to scale more strongly with near-surface stiffness than peak bending, enabling rapid scenario checks.

Taken together, these results close the gap between field testing and fixed-head group design in layered deposits and support more reliable, economical foundations for critical infrastructure on soft or layered soils.

2. Material and methods

2.1. Site description

Nhon Trach 3&4 power plant project is located at the confluence of the Dong Tranh and Long Tau Rivers, within the Ong Keo Industrial Park, Phuoc Khanh Commune, Nhon Trach District, Dong Nai Province. The soil conditions at the project site are summarized as follows while the soil profile is shown in Fig. 1:

Layer SL: Loose sandy soil (yellowish grey). Thickness 0.3–3.2 m, average SPT = 10.

Layer 1: Soft clay and organic mud. Thickness 2.7–10.7 m, average SPT = 1.

Layer 1b: Firm sandy clay. Thickness 0–2.0 m, average SPT = 7.

Layer 2: Stiff clay. Thickness 6.3–26.1 m, average SPT = 13.

Layer 2a: Dense fine sand layer interbedded within Layer 2. Thickness 0.6–8.0 m, average SPT=16.

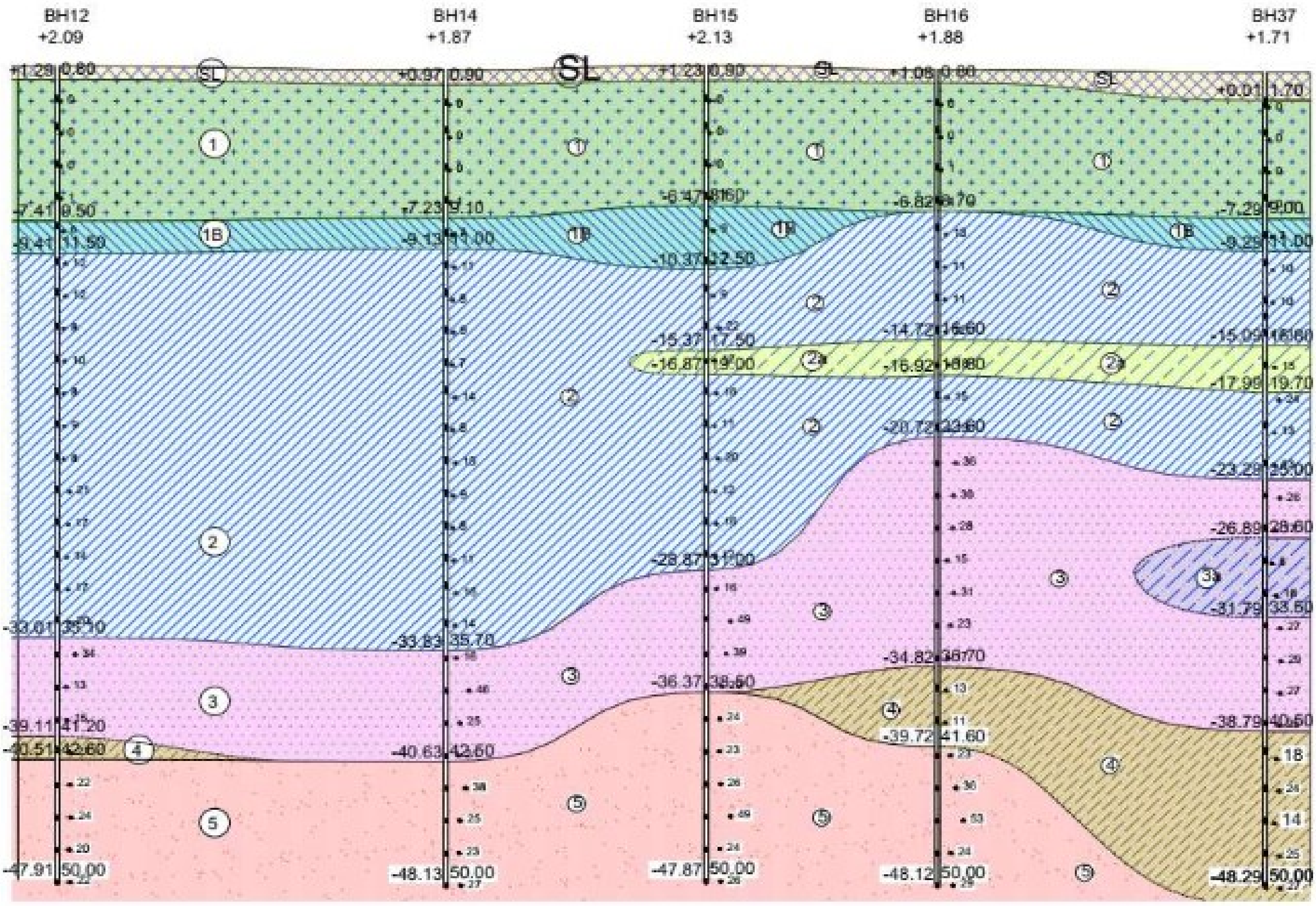

Fig. 1. Soil profile

Layer 3: Dense clayey sand. Thickness 1.8–25.5 m, average SPT = 24.

Layer 3a: Very stiff clay. Thickness 0.3–8.6 m, average = 3.2 m.

Layer 4: Stiff to very stiff sandy clay. Thickness 1.4–21.9 m, average SPT = 18.

Layer 5: Medium dense fine sand. Thickness 0.5–31.4 m, average SPT = 26.

It should be clarified that the power plant area was backfilled with sand with a minimum compaction requirement of K90 up to the design elevation of +2.483 m. Therefore, the Power Block area of the project will have an upper sand layer with a thickness of approximately 3.0 m.

The Nhon Trach 3&4 Combined Cycle Power Plants utilize D300 and D400 Class A piles for minor structural components, while D500 Class B piles are used for major structural elements requiring high lateral load capacity, such as steam turbine and gas turbine foundations or deep excavation items. The properties of pile are summarized in Table 1.

Table 1. PHC pile parameters

No	Pile diameter (mm)	Pile class	M crack (kN.m)	M ultimate (kN.m)
1	300	A	24.5	36.7
2	400	A	54.0	81.0
3	500	B	147.2	265.0

2.2. Full-scale field testing

In this project, full-scale field tests were performed to determine the ultimate lateral bearing capacity of prestressed high-strength concrete (PHC) piles with diameters of D300, D400, and D500 [11]. The experimental results provide a basis for future numerical modeling and comparative analysis. The testing followed the procedure outlined in ASTM D3966 [12]. For each pile, the load was applied in incremental and decremental stages using a hydraulic jack, with each load step maintained for a defined duration to ensure equilibrium. Measurements of lateral displacement, applied load, and elapsed time were recorded immediately before and after each load increment.

Fig. 2. Installation diagram of lateral test pile

The testing was concluded when one or more of the following conditions were observed: (1) structural failure of the pile, (2) circumferential cracking around the pile shaft, or (3) lateral displacement exceeding 10% of the pile diameter. All tests were conducted under free-head conditions, meaning the top of the pile was unrestrained and no vertical load was applied.

Lateral loads were applied horizontally using a hydraulic jack, which reacted against a system of concrete blocks serving as anchors. A schematic representation of the test setup, along with field photographs, is provided in Fig. 2. Technical specifications of the testing equipment are summarized in Table 2.

It should also be noted that this study was conducted in the power block area, where only a limited number of piles/pile groups were considered. This increases sampling error and limits broad generalization. To mitigate bias, we (i) strictly followed ASTM D3966 test procedures; and (ii) calibrated the numerical model to reproduce both the head load–displacement (H–u) curve and the bending-moment distribution along the pile shaft.

Moreover, the field tests were performed only under free-head conditions, whereas the in-service condition is fixed-head (through pile fixity via the pile cap/foundation). The free-head configuration at the pile head was selected to (i) directly measure the H–u curve with minimal boundary interference from the superstructure and (ii) ensure safety and practical feasibility of instrumentation. The 3D Plaxis model was then calibrated to match the free-head H–u curve and the observed crack-initiation load. On that basis, boundary-condition translation simulations, a procedure that uses a field-calibrated 3D model built from free-head test data to infer the response of fixed-head/pile-group configurations for practical design, were carried out for fixed-head and pile-group scenarios (fixity through the cap/foundation) to estimate the actual in-service response. This approach allows free-head field data to be extrapolated to the structural configuration while maintaining error control through the above calibration criteria.

Table 2. List of test equipment

No	Equipment	Technical specification
1	Hydraulic jack	Capacity: 2,105 kg
2	Hydraulic pump	Maximum pressure: 69,106 Pa
3	Pressure gauge	Measuring capacity: 0-60.106 Pa
4	Dial gauge	Max stroke: 100 mm
5	Reference beam	Length: 6 m

In addition, only head displacement and crack observations were recorded in the field; shaft stresses were not measured. This reflects common instrumentation/cost constraints, as many lateral load campaigns do not employ strain gauges. The gap can be addressed by a multi-criteria validation that does not require direct stress measurement: (a) matching the head H–u curve; (b) comparing the crack-initiation load H_{cr} observed in the field; and (c) checking mechanical consistency between the observed H_{cr} and the calculated cracking condition from the pile's material and section properties. In the simulations, crack initiation is identified when the principal tensile stress at the extreme fiber reaches f_t or when the tensile strain reaches f_t/E_c. The corresponding load is compared with the field H_{cr} for consistency. When H_{cr} cannot be unambiguously located on the H–u curve, a practical criterion is the first break in slope combined with visual crack observation. This procedure enables mechanically sound validation without direct stress measurements while tightly linking field crack observations to the simulation's crack prediction.

2.3. Analytical analysis

At the Nhon Trach 3&4 power plant project, the substructure design adopted the Japanese Standard (JRA) to ensure compatibility and consistency with the superstructure, which was also designed according to Japanese specifications. In accordance with the Japanese Road Association (JRA) guidelines, the lateral displacement at the pile head is calculated as follows [13]:

$$\delta = \frac{H}{2EI\beta^3} \tag{1}$$

where:

δ is the lateral displacement at the pile head (mm),

H is the applied lateral load (N),

E is the Young's modulus of the pile (N/mm^2),

I is the moment of inertia of the pile (mm^4),

β is the characteristic value of a pile (mm^{-1}), which is determined as follows:

$$\beta = \sqrt[4]{k_H \frac{D}{EI}} \tag{2}$$

where:

D is the diameter of the pile (mm) and

k_H is the coefficient of horizontal subgrade reaction (), which is defined as follows:

$$k_H = k_{H_0} \frac{B_H}{0.3} \tag{3}$$

Here, k_{H_0} represents the primary horizontal subgrade reaction coefficient; and B_H denotes the equivalent width of foundation loading (m). These two parameters are determined from the following expressions:

$$k_{H_0} = \frac{\alpha E_0}{0.3} \tag{4}$$

$$B_H = \sqrt{\frac{D}{\beta}} \tag{5}$$

In the Eq (4), E_0 is the deformation modulus of the ground, and α is a correction factor that depends on the type of soil.

Maximum bending moment of pile under lateral force is calculated as follows:

$$M_{max} = 0.3224 \frac{H}{\beta} \tag{6}$$

Iterative process to solve β

Step 1: Initialize β_0 from an equivalent-soil estimate (from CPT/SPT) and/or JRA look-up for a sand-over-clay profile.

Step 2: Compute the theoretical H–u curve (analytical/JRA) with βi; extract the initial tangent slope:

$$K_{h0}^{(i)} = \frac{dH}{du}\Big|_{u\to 0} \tag{7}$$

Step 3: Update β\betaβ using the beam-on-elastic-foundation relation $\beta \sim (k_h/EI)^{1/4}$ so that $K_{h0}^{(i)}$ matches the measured initial slope (or that from the calibrated FEM).

Step 4: Iterate until convergence $|\beta_{i+1} - \beta_i|/\beta_i < 1$ and the secant error at a reference load (e.g., $H = H_{serv}$) is <5%. In practice, convergence was reached in 3–5 iterations for this dataset.

Mechanics of the power-law relations for u_o-E

Consider an elastic beam with stiffness EI on a distributed lateral spring with equivalent stiffness k_h (Winkler / linearized p–y at working strains). The characteristic length is

$$l = \left(\frac{EI}{k_h}\right)^{1/4} \tag{8}$$

For a head lateral load H, the characteristic head displacement scales as

$$u_0 \sim \frac{H}{k_h \cdot l^3} \Rightarrow u_0 \propto k_h^{-3/4} (EI)^{-1/4} \tag{9}$$

The peak bending moment scales as

$$M_{max} \sim H \cdot l \Rightarrow M_{max} \propto k_h^{-1/4} (EI)^{1/4} \tag{10}$$

When the sand cap controls the working stiffness, it is reasonable to take $k_h \propto E$ (effective modulus of the cap). Hence,

$$u_0 \propto E^{-3/4}, \quad M_{max} \propto E^{-1/4} \tag{11}$$

2.4. 3D finite element analysis

To assess the lateral load-bearing capacity of the PHC piles, a three-dimensional finite element model was adopted using Plaxis 3D. The loading procedure in the numerical model was designed to replicate the field test conditions as closely as possible, ensuring consistency between simulated and experimental results. At the project site, the soil profile consists of a sand fill layer with an average thickness of approximately 3.0 m. This is underlain by a weak clay stratum (Layer 1), followed by a stiff to hard clay layer (Layer 2), and then alternating fine sand layers (Layer 2a and

Layer 3). The geotechnical properties assigned to these soil layers in the model are summarized in Table 3.

The soil parameters were derived from a combined in-situ–laboratory workflow. For the sand backfill and sand layers (Layer 2a, Layer 3), E_{50}^{ref}, E_{oed}^{ref}, E_{ur}^{ref}, were estimated from SPT/CPT correlations to relative density and effective stress level, then adjusted to match the initial tangent slope of the measured H–u curve (service-level strains). Drained strength parameters ϕ' and dilation ψ were taken from triaxial CD, with hydraulic conductivity k from grain-size/constant-head tests. For the soft clay layers (Layer 1, Layer 2), undrained stiffness was taken from oedometer and CU/UU triaxial results, with ϕ', c' from effective-stress triaxial interpretation and approximately $m \approx 0.5$ consistent with HS recommendations for fine-grained soils. The drainage setting follows soil type and loading rate: sands modeled drained, clays undrained A. Final values were back-checked against (i) the measured initial H–u stiffness and (ii) the depth of maximum bending moment inferred from the numerical model, to ensure consistency of soil layering effects.

PHC piles used on site are factory-produced with tight quality control; the scatter in elastic modulus E_c and cracking strength f_t is limited according to the manufacturer's. Within the tested lateral-load range, the system stiffness is governed primarily by the near-surface sand cap and soil–pile interaction rather than by small variations in E_c. A targeted sensitivity check showed that varying E_c by ±15% changed head displacement by <5%, whereas varying the sand-cap modulus by ±20% altered head displacement by about 15–25% and the location of M_{max} slightly confirming soil dominance. Consequently, pile-material variability was not parameterized in the baseline model; pile capacity was instead verified separately using the section cracking/bending limits (i.e., $M_{cr}=f_tW$), which remained above the demand in the analyzed cases.

2.4. Details of the Plaxis 3D model

Table 3. Soil parameters

	Filling sand	Layer 1- Soft clay	Layer 2 Stiff clay	Layer 2a Fine sand, medium dense	Layer 3 Fine sand, dense to medium dense
Model	Hardening soil	Hardening soil	Hardening soil	Hardening soil	Hardening soil
Drainage	Drained	Undrained A	Undrained A	Drained	Drained
γ (kN/m^3)	18.5	14.3	18.5	18.0	19.0
e	0.70	2.38	0.85	0.80	0.65
E_{50}^{ref} (kPa)	8,000	4,415	10,653	20,000	30,000
E_{oed}^{ref} (kPa)	8,000	4,415	10,653	20,000	30,000
E_{ur}^{ref} (kPa)	24,000	13,244	31,958	60,000	90,000
m	0.5	0.9	0.9	0.5	0.5
c' (kPa)	1.0	5.0	19.0	0.0	0.0
φ' (degree)	28.0	22.7	25.0	32.0	35.0
k (m/day)	0.1	1.4E-05	1.9E-05	0.1	0.1

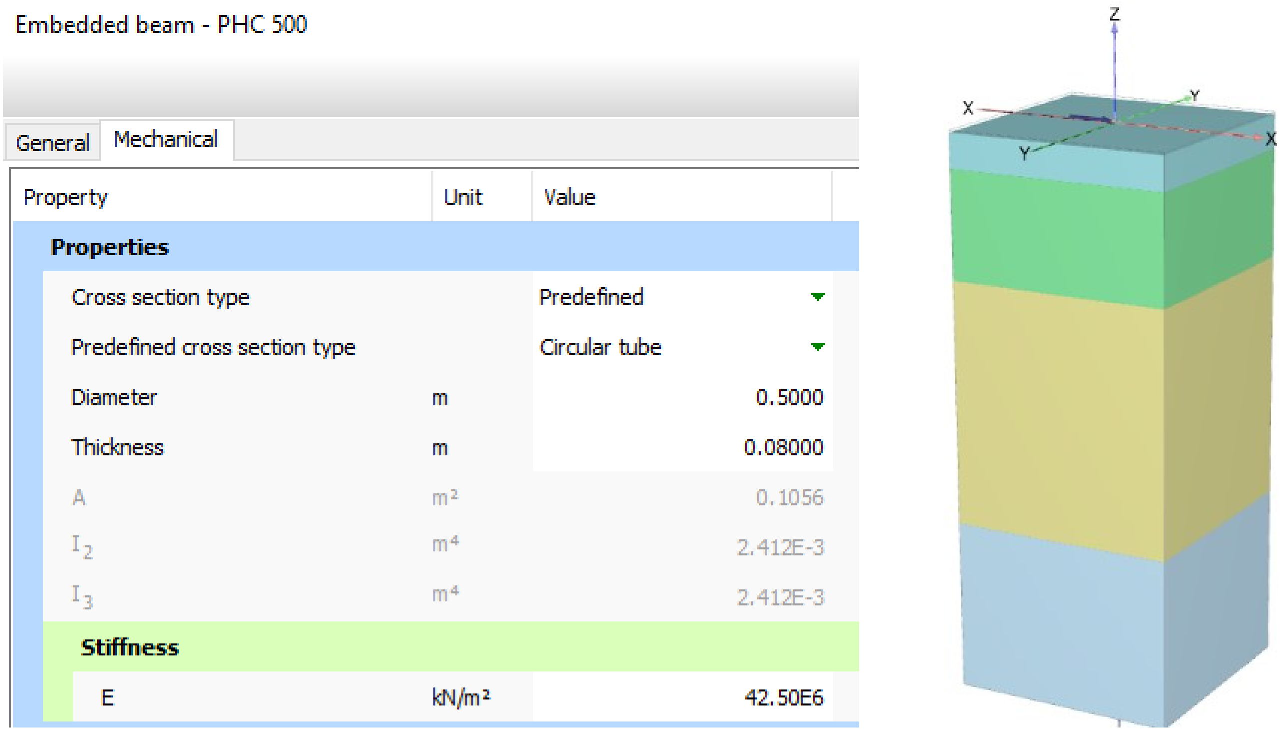

Fig. 3. Plaxis 3D model

A computational domain of 20 × 20 × 50 m was adopted around the pile group to reduce boundary reflections. The 3D domain 20×20×50 m provides a lateral distance to the side boundaries ≥ 40D (with D=0.5 m) and a depth of about 100D, consistent with beam-on-foundation guidance to limit wave reflections and to fix the base.

The base was fully fixed in all directions (ux=uy=uz=0). The side boundaries used "roller" conditions (normal displacement fixed, tangential slip permitted) to avoid constraining lateral deformation. Lateral load was applied incrementally following the field loading schedule; convergence was checked using Plaxis's energy norm criterion.

The standard Plaxis mesh was employed with local refinement around the pile shafts and within the ~3.0 m sand cap to capture strain gradients; element density was gradually coarsened away from the piles. A convergence checking indicated that adding one refinement level or enlarging the domain by 10 m changed the head displacement and M_{max} only by a few percent.

The model was calibrated to reproduce both the head load–displacement (H–u) curve and the crack-initiation load observed in the field. Additional comparisons with JRA were performed to establish a conservative reference for displacement. Consistency with classical analytical solutions (Broms [14] and Poulos [15]) after equivalent-soil conversion, which showed consistent trends for H-u curve. These validations support the model's reliability for parametric analyses and for boundary-condition translation from free-head to fixed-head/pile-group configurations.

The PHC piles were modelled using embedded pile elements, a line-type element representing the pile shaft that is "embedded" in the 3D soil mesh; it transmits axial force, lateral force, and bending moment through contact parameters, without explicitly modeling a borehole/solid pile geometry. It allows for a realistic simulation of pile-soil interaction. The pile geometry and material characteristics used in the model are shown in Fig. 3. The D500 PHC pile was modeled with a length of 25.6 m, corresponding to the actual installation depth at the site. The mesh consists of 5,442 finite elements and 9,160 nodes, providing a sufficiently refined discretization for accurate analysis. The pile was modeled based on its actual geometric parameters (diameter, wall thickness, and moment of inertia) and material properties as specified by the manufacturer.

The pile test results were documented in the report, and displacement graphs were plotted for each load increment. Fig. 4 illustrates the relationship between applied load and pile head displacement.

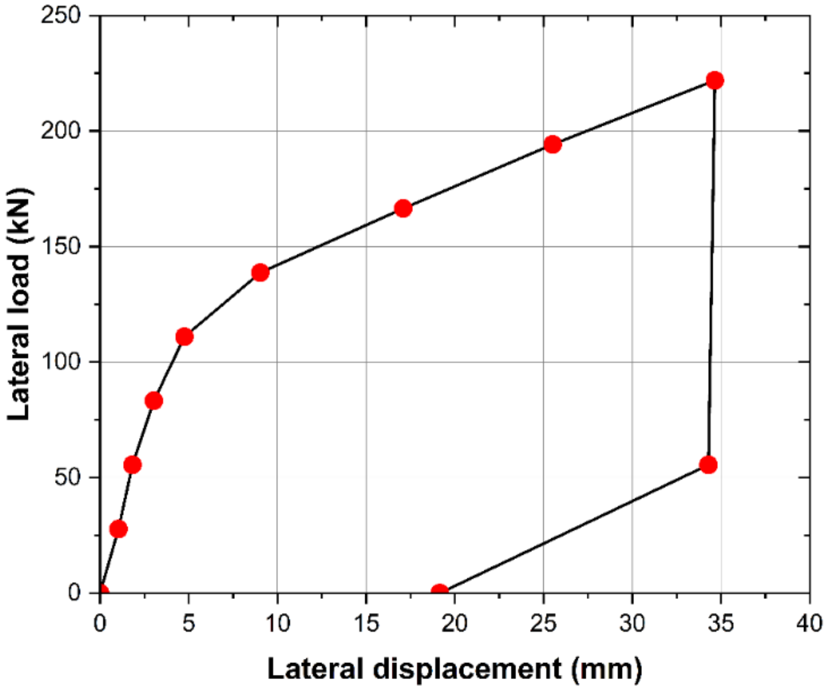

Fig. 4. Diagram of lateral test pile (pile L500-1)

Table 4. Summary of pile test results

Pile test No.	Actual of pile pressing length in Ground	Pressing load	Max. test load	Displacement at Max. test load	Remarks
	(m)	(kN)	(kN)	(mm)	
L500-01	25.64	4,260	222	34.66	Cracks observed around pile at max load
L500-02	31.94	3,526	222	29.01	
L400-01	16.24	983	162	31.82	
L400-02	22.60	1,151	162	28.16	
L300-01	22.24	1,511	88	37.53	Cracks observed at 88 kN; displacement > 10%D (30 mm)
L300-02	28.00	983	99	30.46	Cracks observed at 99 kN; displacement ≈ 10%D (30 mm)

The lateral bearing capacity of piles depends on both the bearing capacity of the pile material and that of the surrounding soil. In terms of material, the piles are manufactured in a factory using high-strength concrete, ensuring excellent quality control. This study will not consider the effect of material on the lateral bearing capacity of piles. The material parameters of the piles are taken from the manufacturer's catalog. The cracking moment and ultimate moment values for each pile type are presented in Table 2.

The summarized results of the lateral load tests for piles with diameters D500, D400, and D300 are presented in Table 4. The pile length is determined when the pile reaches the designed pressing force.

3. Results and Discussion

3.1. Lateral bearing capacity of PHC pile

The displacement and internal force results of pile L500-1 at the maximum applied load of 222 kN are presented in Fig. 5. The results in Fig. 5 indicate that at a load level of 222 kN, the corresponding pile head displacement is 30.9 mm, and the bending moment in the pile reaches 222.8 kNm/m. This value exceeds the cracking moment (M_{crack}) of the D500B pile, leading to cracking at this load level. The analysis further reveals that both displacement and bending moment gradually approach zero at a depth of approximately 4.5 m. The measured lateral load–pile head displacement (H–u) responses for the three pile types (D500, D400, and D300) are presented in Figs. 6 to 8, together with the corresponding Plaxis 3D predictions and the JRA analytical results.

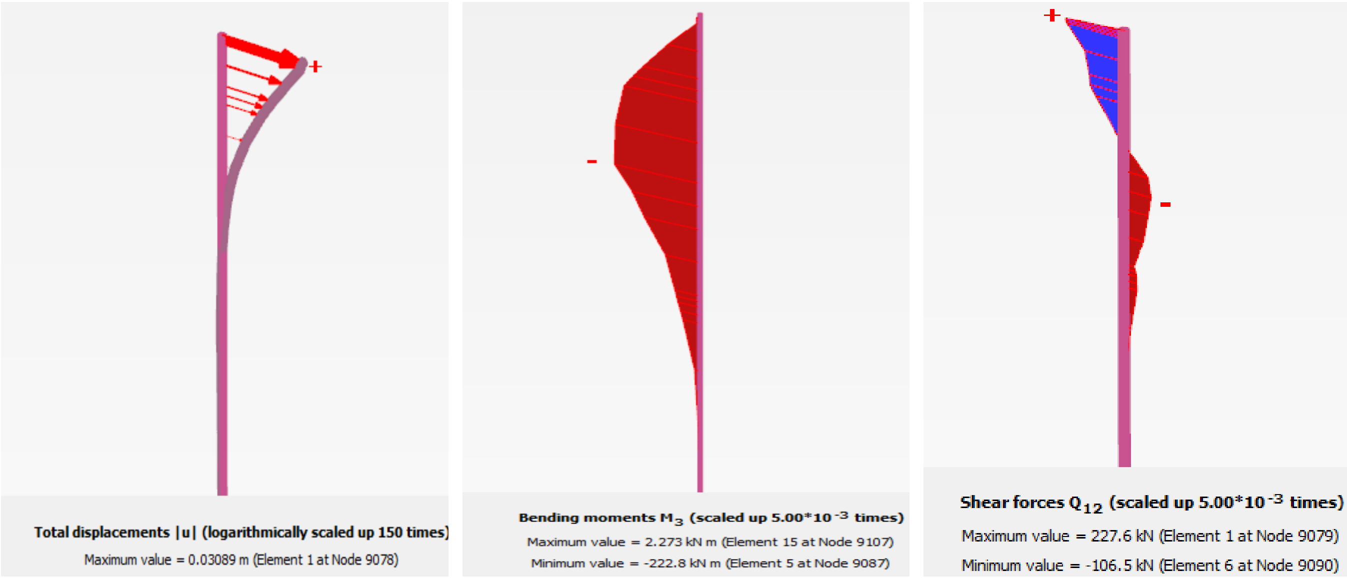

a- Pile displacement b- Bending moment c- Shear force

Fig. 5. Analysis results of pile L500-01 using the Plaxis 3D model

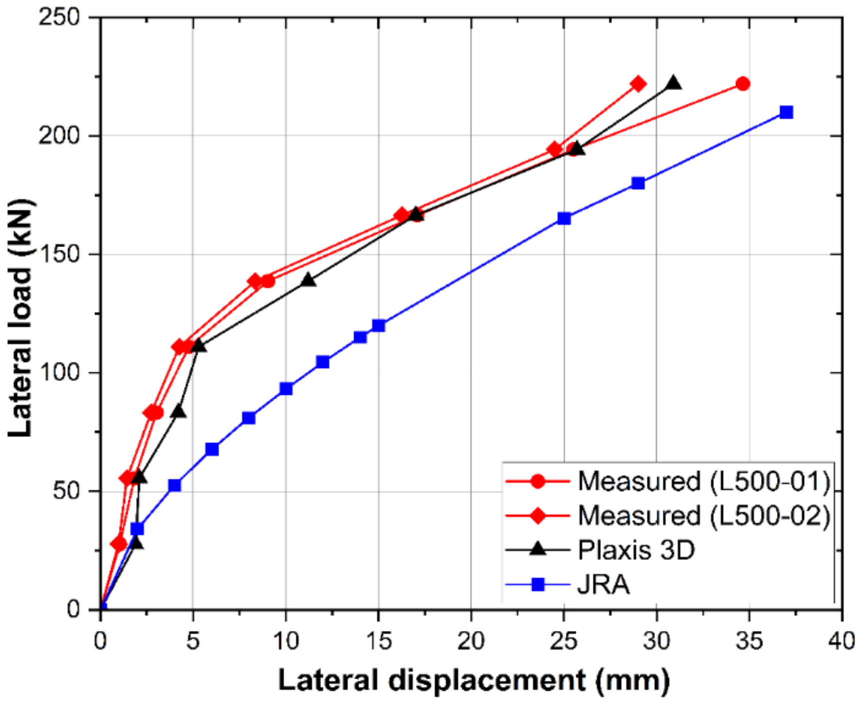

Fig. 6. Comparison of the analysis results for D500 piles (L500-01 and L500-02)

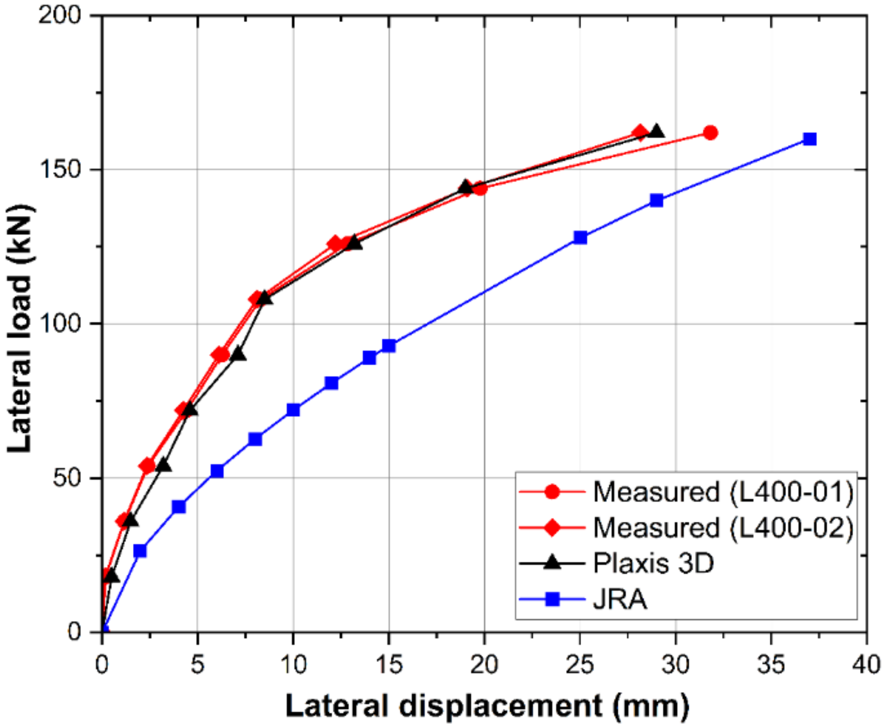

Fig. 7. Comparison of the analysis results for D400 piles (L400-01 and L400-02)

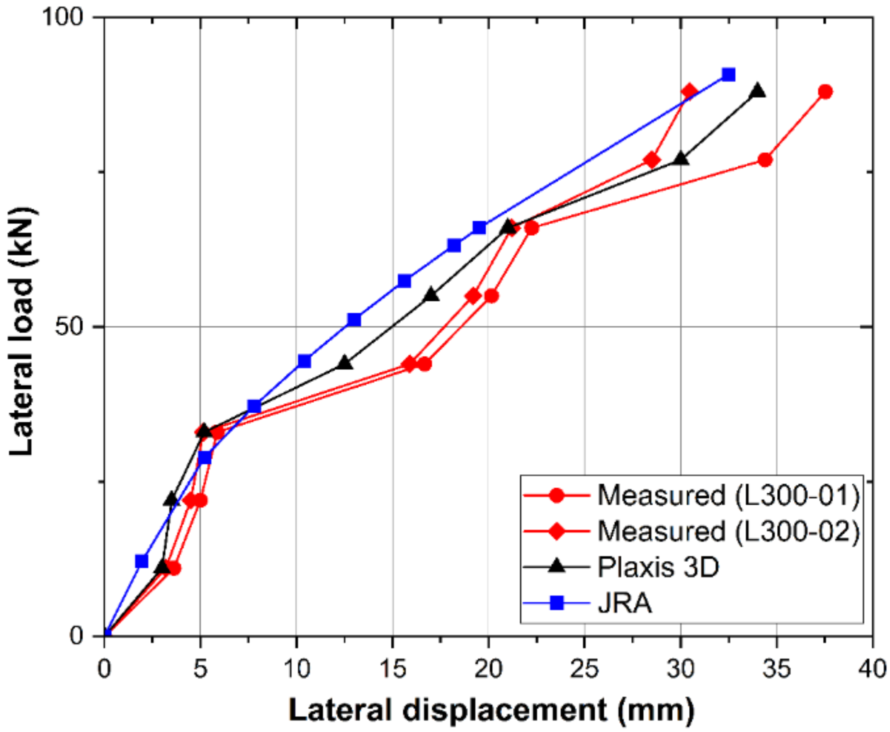

Fig. 8. Comparison of the analysis results for D300 piles (L300-01 and L300-02)

The comparison results show that the displacement trends and values of the piles under lateral loading are consistent between the experimental data and the Plaxis 3D model. Therefore, the numerical model demonstrates high reliability. Based on the experimental and numerical model results, it can be confirmed that the pile head displacement exhibits a nonlinear relationship with the applied lateral load. This finding is consistent with previous studies by Zeng et al. [6] and Shengnan et al. [7].

To facilitate comparison with previous full-scale studies, the head displacement is normalized by pile diameter (u/D). The mobilized u/D at maximum load for each test is summarized in Table 5, showing values of approximately 0.06–0.13. These levels are comparable in order of magnitude to full-scale lateral load tests on precast concrete piles reported in the literature [16]. In the present case, the observed differences in curve shape and stiffness evolution among D500–D400–D300 piles can be attributed to the layered ground profile and the free-head boundary condition adopted in the field test, which affects the mobilized moment distribution and the apparent head stiffness in the early loading stage. This trend is consistent with the classic p–y interpretation for layered ground, where a stiffer near-surface layer governs the initial response while deeper soft clay increasingly controls the large-displacement behavior (Matlock [4]; and Reese et al. [17]).

When displacement is normalized by pile diameter (u/D), the working-range u/D falls below the envelope of standard p–y models for an ideal free head but is close to published full-scale lateral tests on single piles in layered soils. This is reasonable because, although our field setup was nominally free-head, a small residual rotational restraint from the reaction frame and clamping plates slightly increased the initial stiffness relative to the ideal free-head assumption, an observation often reported in full-scale tests. Compared with classical analytical solutions [14, 18] for homogeneous sand/clay, our initial H–u slope lies between the sand and clay bands due to the sand cap effect; as load increases, the curvature of H–u reflects greater participation of the soft clay, consistent with the conclusion that layered stratigraphy causes the H–u curve to soften at higher load levels.

Table 5. Normalized pile head displacement at maximum test load

Test ID	Max. test load H_{max} (kN)	Displacement at H_{max}, u (mm)	u/D
L500-01	222	34.66	0.069
L500-02	222	29.01	0.058
L400-01	162	31.82	0.080
L400-02	162	28.16	0.070
L300-01	88	37.53	0.125
L300-02	99	30.46	0.102

Furthermore, Figs. 6–8 show that the JRA prediction does not reproduce the measured H–u curves as closely as the calibrated 3D FE model, and the degree of conservatism is not uniform across pile diameters and displacement ranges. To place the comparison on a consistent basis, Table 5 summarizes the normalized pile head displacement (u/D) mobilized at the maximum test load for each field test. The values indicate that the tests reached u/D≈0.058–0.069 for D500, 0.070–0.080 for D400, and 0.102–0.125 for D300 at the applied H_{max} levels. These deformation levels confirm that the response assessed in Figs. 6–8 extends well into the nonlinear range, where differences between simplified analytical assumptions and site-specific behavior are expected to become more apparent (in Table 5).

For the D500 and D400 piles, the JRA curve generally predicts larger head displacement than both the field measurements and the calibrated Plaxis 3D simulations for the same lateral load, particularly in the practical displacement range used for interpretation of lateral performance. This trend implies that, when the JRA approach is used in a displacement-based check, it tends to be conservative for the larger-diameter PHC piles at this site. A key reason is the layered ground condition at Nhon Trach, where a relatively stiff sand cap overlies softer clay. For larger diameters, the near-surface stress and strain field contributing to lateral resistance is more strongly influenced by the stiffer upper layer at small-to-moderate displacements, resulting in higher apparent initial stiffness and greater resistance mobilization than would be captured by an equivalent-soil idealization. In other words, the field and FE curves reflect a stiffer early response that the JRA reduction procedures do not fully represent under layered conditions. In addition, while the test setup was designed to apply free-head loading, practical boundary effects such as minor fixture compliance and unavoidable residual restraint can slightly steepen the initial slope of the measured H–u response compared with the idealized free-head condition embedded in the JRA formulation; this influence is most visible at small displacements, which then propagates into the perceived conservatism of the JRA curve at a given load level. Finally, the JRA p–y formulation and its diameter scaling are calibrated to broad soil categories and simplified profiles; under strongly layered stratigraphy and stress-dependent stiffness behavior, the analytical curve can remain conservative for larger diameters because it cannot explicitly represent (i) the stress-level dependence of stiffness around the pile head and (ii) the progressive mobilization of confinement and interface effects that increase lateral resistance beyond tabulated bounds.

For the D300 piles, the overall agreement between JRA and the measured/FE curves is closer at larger displacements; however, it should not be interpreted as a perfect match over the entire loading history. As seen in Fig. 8, deviations can occur at intermediate displacements even if the curves become similar near the upper end of the displacement range. This behavior is consistent with the mechanics of smaller-diameter piles: their lower flexural rigidity leads to a more rapid involvement of deeper soil strata relative to diameter, so the influence of the underlying softer clay is mobilized earlier as displacement increases. Under such conditions, the “equivalent” representation inherent to JRA can become closer to the effective site response at larger u/D levels, which is also reflected by the larger normalized displacements achieved in the D300 tests ($u/D \approx 0.102$–0.125 at H_{max}) as shown in Table 5. Therefore, the apparent near-agreement for D300 should be stated as a displacement-range-dependent observation rather than a general statement for all stages of loading.

From a practical design perspective, the above comparison suggests that the JRA method can be used as a rapid screening tool, especially when only preliminary estimates are required; however, for layered ground profiles similar to Nhon Trach and for larger PHC pile diameters (D400–D500), the calibrated 3D FE model provides a more reliable representation of the measured lateral response and should be preferred for working design and for interpreting free-head test results under fixed-head or group-foundation boundary conditions. More broadly, the results emphasize that lateral load capacity and deformation are controlled not only by pile diameter and material properties but also, and often dominantly, by geotechnical parameters, particularly the stiffness and thickness of the upper soil layer and its stress-dependent behavior. So site-specific characterization remains essential when translating field test outcomes into design recommendations.

The H–u curve exhibits high initial stiffness (a linear to near-linear segment as $u \to 0$) governed by the sand cap; as H increases, the curve softens due to mobilization of deformations in the underlying soft clay and/or approach to cracking at the extreme fiber of the pile. In the p–y framework: within the sand cap, the initial p–y stiffness is high and increases with effective stress, producing a steep H–u slope; deeper in the soft clay, the p–y response approaches the ultimate resistance p_u (a plateau), which reduces the equivalent stiffness and softens the H–u curve. The result is consistent with beam-on-elastic-foundation scaling: $u_o \propto k_h^{-3/4}$; and $M_{max} \propto k_h^{-1/4}$ with the cap spring k_h proportional to the effective modulus E, it follows that $u_o \sim E^{-3/4}$ is markedly more sensitive than $M_{max} \sim E^{-1/4}$. This explains why densifying/improving the sand cap yields a pronounced reduction in displacement, whereas changes in peak bending moment are milder. Moreover, boundary-condition translation confirms that increasing head restraint (fixed-head) increases the initial lateral stiffness and shifts the bending-moment demand toward the pile head. Conversely, under free-head conditions the maximum bending moment can be higher for the same lateral load, whereas the difference in head displacement is relatively small; this trend is consistent with the subsequent fixed-head versus free-head numerical comparisons presented later in this section. Accordingly, the following procedure is recommended: (1) calibrate the model using the initial slope and the crack-initiation load Hcr identified via the first slope break plus visual crack detection; (2) check the consistency of the Mmax depth; and (3) use JRA as a lower-bound for displacement where a stiff sand cap exists, applying boundary-condition translation to infer fixed-head/group responses for similar projects.

3.2. Factors influence on the lateral

In this study, the authors varied the modulus of deformation (E) of the 3m-thick filling sand layer from 4,000 kPa to 15,000 kPa. The dependency of pile head displacement and maximum bending moment on the E value is presented in Fig. 9 and Fig. 10, corresponding to the maximum test load specified in Table 2.

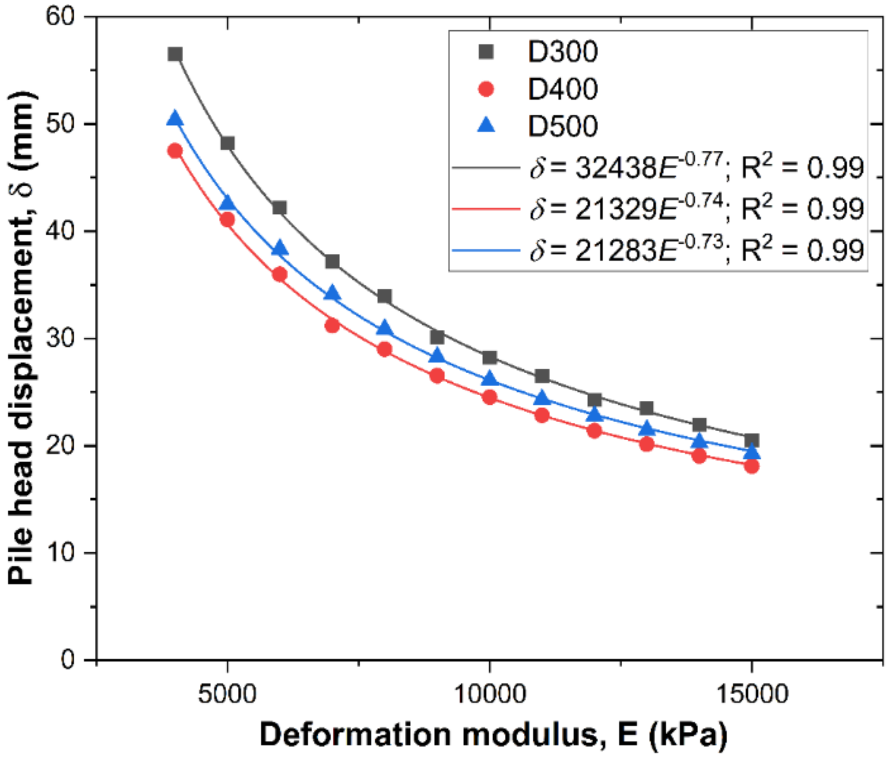

Fig. 9. Dependency of Pile Head Displacement on the Modulus of deformation of the Backfill Layer

The analysis results presented in Figs. 9 and 10 indicate that pile head displacement is approximately inversely proportional to E value following a three-fourths power relationship, while the bending moment is approximately inversely proportional to E following a one-fourth power relationship. This is consistent with the relationship between displacement and bending moment concerning the deformation modulus of the soil foundation, as specified in the JRA standard and presented in equations (1), (2), and (6). These power relations explain why head displacement is far more sensitive to the cap stiffness than peak bending (exponents 3/4 vs 1/4), matching the trends in Figs. 9-10. Moreover, with fixed-head restraint, the initial slope of H–u increases (stiffer boundary), while M_{max} shifts toward the head; under free-head, M_{max} is larger for the same H whereas u_0 does not increase proportionally consistent with beam-on-foundation solutions and field observations.

3.3. Fixed and free head pile displacement

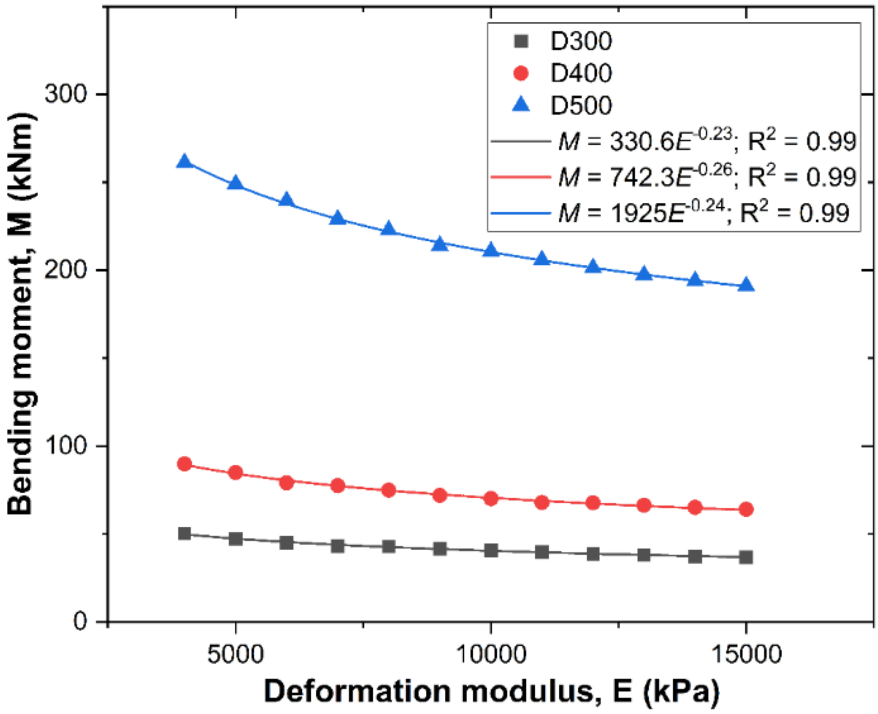

Fig. 10. Dependency of bending moment on the Modulus of deformation of the Backfill Layer

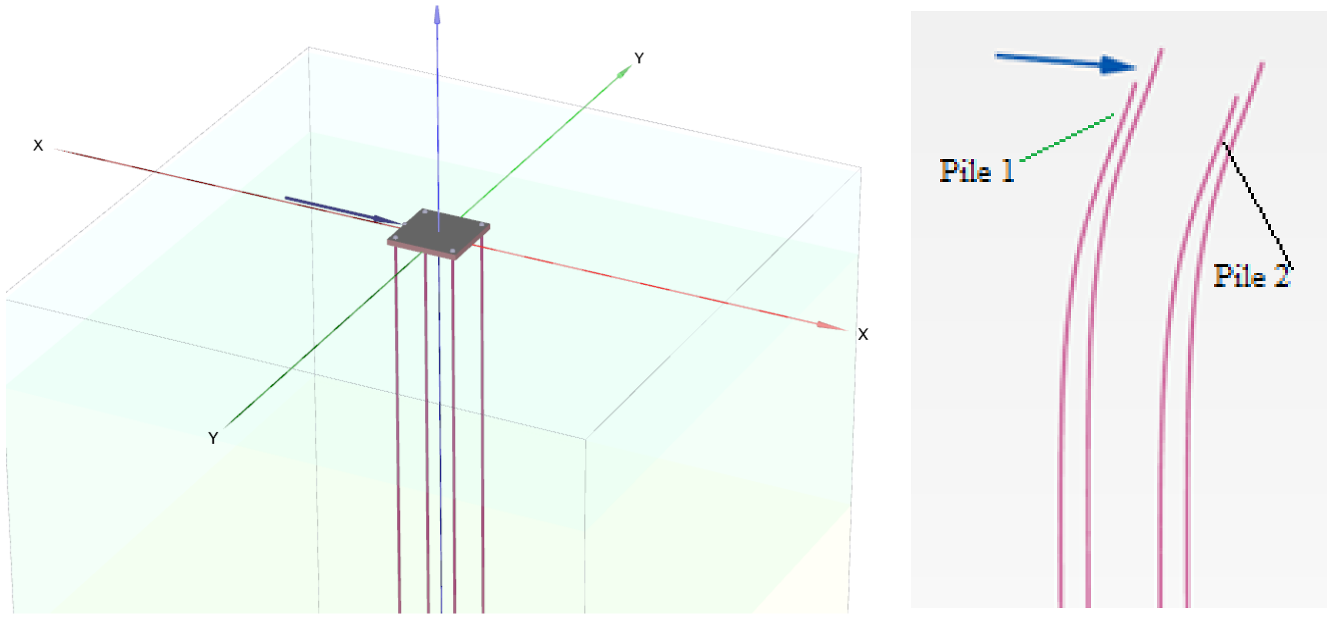

Fig. 11. Model of the Four PHC D500 Piles

It is important to note that foundation systems are typically designed with multiple interconnected piles, meaning that testing a single pile under free-head conditions does not fully represent the actual behavior of the foundation structure. In field experiments, conducting lateral load tests on a pile group is often challenging due to high implementation costs.

To better understand the differences in lateral load-bearing capacity between free-head and fixed-head conditions, the authors analyzed a foundation system consisting of four PHC D500 piles, arranged with a center-to-center spacing of 3D (equivalent to 1.5 m). A lateral load four times greater (888 kN) was applied to this pile group. To minimize the influence of the pile cap on lateral load distribution, the four piles were connected by a thin concrete slab with a thickness of 20 cm. Fig. 11 illustrates the Plaxis 3D model of the four-pile group and the displacement of the pile group under the applied load.

Due to the symmetry of the model, the analysis focuses on two distinct pile positions: Position 1 and Position 2. The differences in displacement and bending moment between the free-head and fixed-head conditions are presented in Figs. 12 and 13, respectively. The comparison of displacement between free-head and fixed-head conditions indicates no significant difference. Piles 1 and 2 in the model exhibit identical displacements due to the rigid connection between the piles.

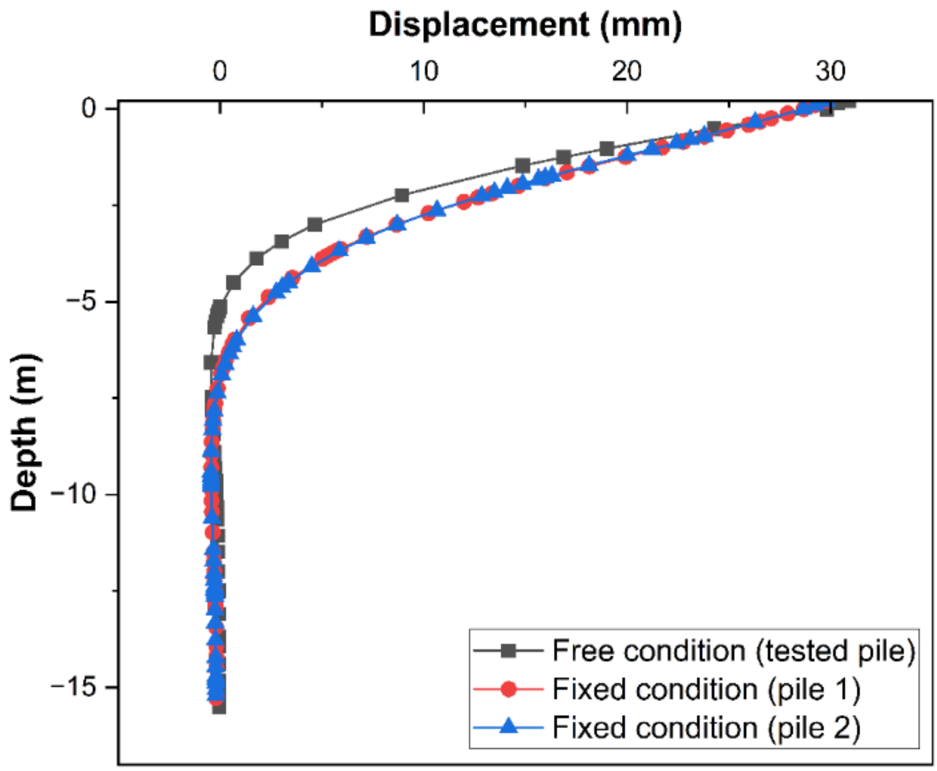

Fig. 12. Comparison of pile displacement between Free-Head and Fixed-Head conditions

The analyses reveal a clear redistribution of bending demand between boundary conditions. Under free-head behavior, the maximum bending moment develops at nearly 3.5 m below the head and vanishes at the pile top; under fixed-head behavior, the peak shifts to the pile head, and the moment at 3.5 m depth is about 12% lower than the peak. On a like-for-like lateral load H, the maximum bending moment is about 17% higher for the free-head case, whereas the difference in head displacement is negligible. Two design consequences follow. First, free-head tests are conservative for material-strength checks (moment/cracking): using free-head data will not underestimate bending demand for fixed-head/group conditions. Second, serviceability by displacement must reflect the actual head restraint; fixed-head systems exhibit a stiffer initial slope of the H-u curve, so translating free-head displacements directly to fixed-head design would be misleading without accounting for head fixity).

These trends are consistent with a p–y interpretation in layered ground with a stiff sand cap over soft clay. The sand cap controls the initial stiffness (steeper H-u slope), while increasing lateral load mobilizes the underlying soft clay, producing the observed curve softening and shifting of the bending maximum with boundary restraint. In this setting, code-type procedures such as JRA tend to be conservative in displacement for larger diameters (D400–D500), yet are near-accurate for smaller diameters (D300) where the influence zone penetrates the soft clay earlier. Practically, this means: (i) use free-head test results as a safe basis for bending checks; (ii) when displacement governs, adopt a fixed-head (rigid cap) model calibrated to field data or apply a documented boundary-condition translation; and (iii) to reduce head displacement, prioritize improving the near-surface stiffness (e.g., densifying/compacting the sand cap), noting that displacement is more sensitive to cap stiffness than peak bending. Collectively, these findings provide design-oriented guidance for PHC piles and pile groups in layered deposits typical of Nhon Trach–type profiles.

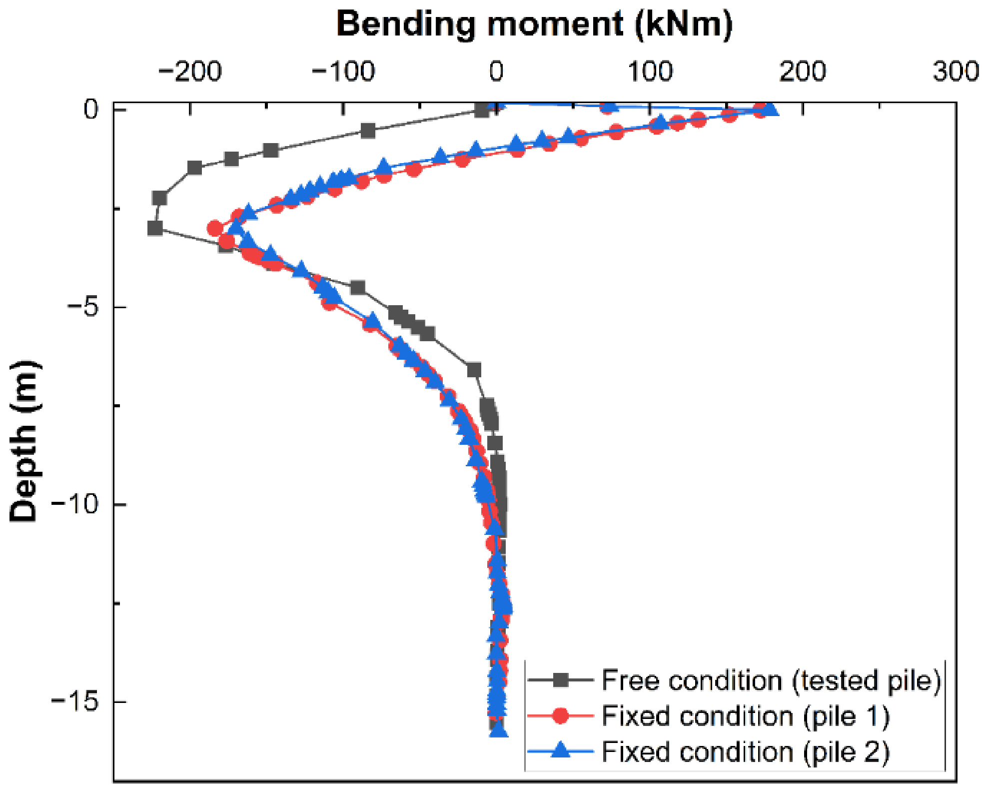

Fig. 13. Comparison of bending moment between Free-Head and Fixed-Head conditions

3.4. Limitations

Despite the scientific and practical contributions, several constraints remain. First, the field campaign was limited to free-head lateral load tests; no measurements were taken for fixed-head/pile-group configurations, shaft stress/strain along depth were not instrumented, and combined axial–lateral (N–H) or cyclic/dynamic loading was not executed. The small sample size further restricts statistical generalization. Second, on the numerical side, the Hardening Soil constitutive law and the embedded pile formulation necessarily idealize soil–pile interaction: local gap formation and slip, cyclic degradation of interface stiffness, and damage of pile material were not modeled explicitly. In addition, hydrological/time-dependent conditions (e.g., groundwater fluctuations, post-construction consolidation) were not monitored and thus not reflected in stiffness calibration. Third, potential numerical errors persist: the chosen domain (about 20×20×50 m) and mesh refinement were selected for tractability; however, boundary effects and mesh sensitivity can still bias head displacement and peak bending by a few percent, particularly at higher load levels. Consequently, the findings are most applicable to layered deposits similar to Nhon Trach under predominantly static lateral loading, and should be treated as reference rather than directly extrapolated to substantially different geologies or loading regimes.

Building on these limitations, future work should expand field evidence and reduce modeling idealizations. Priority actions are: fixed-head and pile-group lateral tests should be executed with synchronized head displacement-rotation measurements and depthwise strain instrumentation (strain gauges or FBG) to recover M(x). Combined N-H and cyclic sequences in accordance with ASTM D3966 are recommended. Co-located CPTu/SCPTu, laboratory oedometer and CIU/UU tests, and groundwater monitoring should be incorporated to justify and update E_{50}^{ref}, E_{oed}^{ref}, E_{ur}^{ref}, c’, ϕ’, over time. On modeling, use HSsmall or cyclic-capable models (e.g., PM4Sand/PM4Silt), implement an explicit soil-pile interface to allow gap-slip and cyclic stiffness degradation, and conduct systematic mesh/boundary convergence studies. Cross-validation with LPILE/OpenSeesPL and Bayesian calibration are encouraged to quantify parameter uncertainty and predictive intervals. Finally, develop site-specific p–y curves and boundary-condition translation factors (free-head to fixed-head) for head displacement u and Mmax yielding design-ready guidance for similar layered deposits.

4. Conclusion

Full-scale free-head lateral tests on PHC piles, combined with a calibrated 3D FE model, established a robust basis for interpreting fixed-head and group behavior in layered deposits with a stiff sand cap over soft clay. The analyses confirm close agreement between measurements and simulations in both the initial stiffness and curvature of the H–u response. For D400–D500 piles, JRA predicts larger head displacements than test/FE results, evidencing conservatism under the studied stratigraphy; for D300, JRA aligns well with observations. Under identical lateral load, the free-head configuration develops a maximum bending moment about 17% higher than the fixed-head case, while the difference in head displacement is small. Thus, free-head data are appropriate and conservative for checking pile material strength (moment/cracking), whereas displacement-based serviceability must explicitly reflect head fixity (rigid caps and groups).

Mechanistically, the stiff sand cap governs the initial H–u slope, while mobilization of the underlying soft clay drives nonlinear softening and shifts in bending-moment distribution with boundary restraint. The observed sensitivities are consistent with beam-on-foundation scaling: $u_0 \propto E^{-3/4}$ and $M_{max} \propto E^{-1/4}$, explaining why improving the cap stiffness is markedly more effective for reducing displacement than for reducing peak bending.

The work is bounded by practical limitations: a free-head field program without axial–lateral coupling or cyclic loading, idealized interaction in the HS/embedded-pile formulation, and residual mesh/boundary effects at higher loads. Future efforts should include instrumented fixed-head/group tests, N–H and cyclic sequences, explicit interface modeling with convergence studies, and cross-validation with p–y tools and analytical solutions. Within these limits, the study provides design-oriented evidence and scalable relations to guide fixed-head PHC foundations in layered ground typical of Nhon Trach-type profiles.

References

[1]. L. Hazzar, M. Karray, M. Bouassida, M.N Hussien. (2013). Ultimate Lateral Resistance of Piles in Cohesive Soil. *DFI Journal - The Journal of the Deep Foundations Institute*, 7(1), 59–68. https://doi.org/10.1179/dfi.2013.005

[2]. M. Hetényi. (1946). Beams on elastic foundation. *University of Michigan Press*.

[3]. A.B. Vesić. (1961). Bending of Beams Resting on Isotropic Elastic Solid. *Journal of the Engineering Mechanics Division*, 87(2), 35–53. https://doi.org/10.1061/JMCEA3.0000212

[4]. H. Matlock. (1970). Correlation for design of laterally loaded piles in soft clay. *Offshore Technology Conference, OTC-1204-MS*. https://doi.org/10.4043/1204-MS

[5]. L.C. Reese, W.R. Cox, F.D. Koop. (1974).

Analysis of laterally loaded piles in sand. *Offshore Technology Conference, OTC-2080-MS*. https://doi.org/10.4043/2080-MS

[6]. F. Zeng, C. Jiang, P. Liu. (2023). Cyclic p-y curve model of unidirectional loaded pile in sand considering the characteristic of friction in the strain wedge model. *Ocean Engineering*, 273, 113998. https://doi.org/10.1016/j.oceaneng.2023.113998

[7]. H. Sheng-nan, L. Shan-nan, C. Zhong-xiang, H. Shao-ming. (2013). Test standards for lateral capacity of single PHC pile. *Chinese Journal of Geotechnical Engineering*, 35(zk1), 378–382.

[8]. J. Zhou, E. Oh. (2021). Full-Scale Field Tests of Different Types of Piles: Project-Based Study. *Springer Singapore*. https://doi.org/10.1007/978-981-33-6183-6

[9]. L. Li, X. Liu, H. Liu, W. Wu, B.M. Lehane, G. Jiang, M. Xu. (2022). Experimental and numerical study on the static lateral performance of monopile and hybrid pile foundation. *Ocean Engineering*, 255, 111461. https://doi.org/10.1016/j.oceaneng.2022.111461

[10]. L. Zhang, S. Ahmari. (2013). Nonlinear analysis of laterally loaded rigid piles in cohesive soil. *International Journal for Numerical and Analytical Methods in Geomechanics*, 37(2), 201–220. https://doi.org/10.1002/nag.1094

[11]. Vietnam Macchinery Installation Corporation (LILAMA). IBST–XD LAS 30. (2023). Lateral test report for pile ID L-500-01: Nhon Trach 3 & Nhon Trach 4 power plant project.

[12]. ASTM D3966-07. (2010). Standard Test Methods for Deep Foundations Under Lateral Load. DOI: 10.1520/D3966-07

[13]. Japan Road Association (JRA). (2017). Specifications for Highway Bridges, Part IV: Substructures.

[14]. B.B. Broms. (1964). Lateral Resistance of Piles in Cohesive Soils. *Journal of the Soil Mechanics and Foundations Division*, 90(2), 27–63. https://doi.org/10.1061/JSFEAQ.0000611

[15]. H.G. Poulos, E.H. Davis. (1980). Pile foundation analysis and design. *Wiley*.

[16]. E.G. Burdette, J.B. Tidwell, E.E. Ingram, et al. (2004). Lateral load tests on prestressed concrete piles supporting integral abutments. PCI J 49.

[17]. L.C. Reese, W.F. Van Impe. (2010). Single piles and pile groups under lateral loading. 2nd Edition. *CRC Press*.

[18]. H.G. Poulos, M.F. Randolph. (1983). Pile Group Analysis: A Study of Two Methods. Journal of Geotechnical Engineering, 109(3), 355–372. https://doi.org/10.1061/(ASCE)0733-9410(1983)109:3(355)